Study on the arc behavior and mechanical properties of energy-efficient hybrid CMT-Pulsed gas metal arc narrow gap mild steel welds

Sudheer Kumar Polamuri
Venkaiah Nasina
Basu Biswajyoti
Vinay Deshmuk
Venkata Kiran Degala (dvkiran@iittp.ac.in)
Indian Institute of Technology Tirupati

Research Article

Keywords: Narrow gap welding, P-GMAW, Cold metal transfer, Arc behavior, Metal transfer phenomenon, Mechanical properties

Posted Date: June 26th, 2023

DOI: https://doi.org/10.21203/rs.3.rs-2917065/v1

Version of Record: A version of this preprint was published at The International Journal of Advanced Manufacturing Technology on September 25th, 2023. See the published version at https://doi.org/10.1007/s00170-023-12350-9.

Abstract

The novel hybrid cold metal transfer (CMT) – Pulsed gas metal arc welding (P-GMAW) process was used to perform the narrow gap welding of mild steel plates. A systematic approach was followed to select the working values of numerous process parameters using high-speed images of the welding arc in synchronization with the welding current and voltage. Further, emphasis was given to understanding the influence of pulse frequency on the complex arc and metal transfer behavior in the narrow gap and its subsequent effect on the side wall fusion and mechanical properties of weld joints. The root pass was deposited using CMT process, while the filling and closing passes were deposited using P-GMAW process to minimize the incomplete fusion between the layers keeping the overall heat input lower. A decrease in the narrow gap distance and an increase in the arc oscillation amplitude and welding voltage resulted in severe arc climbing over the facing surface, an inadequate fusion between the layers, and incomplete side wall fusion. Simultaneously decreasing the number of passes and welding speed engendered the overhead flow of the molten pool and hindered the heat transfer from the arc to the already deposited layer resulting in the lack of fusion. Pulse current and duration directly affect the welding arc lengths, resulting in higher welding arc deflections to the side walls in the case of lower pulse frequencies. The controlled welding arc deflections, molten metal transfer, and inter-pulse cooling displayed a noticeable effect on the mechanical properties of the weld joint.

1. Introduction

Thick plates are used to build massive advanced structures in heavy fabrication industries. The joining of thick plates is generally performed using conventional one-sided single V or U butt joints and double-sided V or U butt joints, which entail high costs of workpiece edge preparation, filler material, and weld time. In contrast, narrow gap welding (NGW) is a high-efficiency welding technique with distinctly low heat input and filler material, resulting in a narrow heat-affected zone (HAZ), low thermal stresses, and minimum distortions. The pulsed GMAW (P-GMAW) process is commonly used in the NGW to optimize the heat input to achieve quality weld joints [1]. The recently developed advanced short circuit variant of the GMAW process, Cold Metal Transfer (CMT), can further reduce the heat input over the P-GMAW for a given deposition. Adopting the hybrid CMT - P-GMAW allows optimization of the heat input to achieve superior-quality welds with minimum weld distortions. The hybrid CMT - P-GMAW process in the present work refers to depositing a few passes in the narrow gap joint using the CMT process and the remaining through the P-GMAW process. However, if not appropriately controlled, complex arc behavior and metal transfer phenomenon in CMT and P-GMAW result in welding defects like improper side wall fusion, porosity, inclusion, incomplete fusion, and center line cracking. Further, numerous process parameters associated with CMT and P-GMAW processes enhance the complexity in realizing its influence on weld quality. A systematic study on the effect of the CMT and P-GMAW process parameters on the behavior of arc and metal transfer phenomenon in the NGW and its subsequent control on the weld quality is needed to adopt the Hybrid CMT - P-GMAW NGW technology successfully.

Agarwal et al. [2] employed the P-GMAW method to conduct NGW with a single seam per layer. A hypothetical dimensionless factor (ø) was proposed to study the influence of pulse current, base current, base current duration, and frequency. Better mechanical characteristics of the weld joint were reported at a higher mean current and ø at a lower heat input. It was also observed that the joint quality could be improved by single seam per layer multipass narrow gap P-GMAW by altering the pulse parameters without changing the heat input [1]. Anant et al. [3] used the P-GMAW method with a newly developed GMAW narrow torch nozzle to create an ultra-narrow multipass weld. The impact of gas flow rates on weld joint quality was investigated. Krampit et al. [4] investigated the pulsed arc welding parameters' impact on forming a narrow gap's root layer. It was reported that the increasing pulse current time and decreasing pulse amplitude and frequency resulted in deeper penetration. Zhang et al. [5] investigated the arc properties in the narrow gap GMAW process. The decrease in the arc length was explained while moving from the center pass to the weld passes near the left and right faying surfaces.

Wang et al. [6] employed an arc rotation technique to enhance sidewall penetration in NGW. The increase in rotation speed was observed to have improved the melting rate of wire in the rotation arc NG-GMAW process. Guo et al. [7] described the flow of molten metal in the direction of the weld width during the rotating arc narrow gap horizontal welding process. It was reported that the temperature distribution towards the sidewall was more significant in the rotating arc than in the non-rotational arc, which aids in complete sidewall fusion. In another study, Guo et al. [8] explored the influence of rotating arc frequency on droplet transfer stability. They noticed that a wire rotation frequency of 5–20 Hz results in steady droplet transfer, whereas a frequency of 50 Hz results in unstable droplet transfer.

Liu et al. [9] investigated the effect of active gases on the molten electrode droplet transfer and arc behavior in NG-GMAW. They observed that adding CO_2 to the Ar shielding gas resulted in projected spray transfer and that adding O_2 resulted in slag deposition on the weld surface. Similarly, Cai et al. [10] studied the effect of shielding gas composition in NG-GMAW and found that Helium had a significant role in expanding the weld profile and improving sidewall penetration. In another study, Sun et al. [11] observed that increasing the N_2 percentage of an Ar-based shielding gas improved weld penetration and weld area. It was also observed that using N_2 as the shielding gas might reduce porosity in laser welds. Similarly, Zhao et al. [12] and Wong et al. [13] found that lowering the CO_2 level in the ternary shielding gas ($Ar + CO_2 + O_2$) resulted in a wider arc and a more stable pulsed streaming spray in P-GMAW.

In various approaches to enhance the NGW quality, Zhu et al. [14] introduced flux strips to reduce the arc climbing effect in ultra-NGW, and Xu et al. [15] performed tandem NG-GMAW and explained the influence of wire distance and bent angle of contact tip to get defect free joint. Wang et al. [16] proposed an alternative magnetic field to deflect the pulsed current, allowing a more significant proportion of the arc profile to remain attached to the sidewall to avoid incomplete side wall fusion.

In summary, the application of the hybrid CMT - P-GMAW process for the narrow gap joining of thick steel plates are not reported in the open literature. Further, the studies on the individual effects of the GMAW process parameters on the arc behavior and joint quality in a narrow gap joint are not reported. In the

present work, systematic studies are undertaken to realize the influence of the CMT and P-GMAW process parameters on the behavior of arc and metal transfer phenomenon in the narrow gap joint of mild steel plates and its subsequent impact on the weld bead profiles. Emphasis was given to understanding the effect of pulse frequencies in the hybrid CMT - P-GMAW process on the microstructure and mechanical properties of the narrow gap joints of mild steel plates.

2. Experimental setup

Mild steel plates of 200 mm x 65 mm x 12 mm are used as the base metal, and ER70S-6 wire of diameter 1.2 mm as filler wire in the present study. Table 1 presents the base metal and filler wire chemical composition. Figure 1(a) schematically represents the welding setup consisting of a current sensor and high-speed camera integrated into the welding power source and data acquisition (DAQ) system. The above arrangement yields real-time current and voltage in synchronization with high-speed arc images during the welding operation. Figure 1(b) shows the joint configuration of the welding plates with copper backing. The circular groove in the copper backing ensures complete fusion during the root pass.

Table 1
Composition of base metal and filler wire (wt %)

Elements	C	Mn	Si	P	S	Cr	Cu
Base metal (Mild steel)	0.22	0.49	0.47	0.005	0.01	0.1	0.01
Filler wire (ER70S-6)	0.06–0.15	1.4–1.85	0.8–1.15	0.025	0.035	0.15	0.5

Figure 2 depicts the systematic representation of the procedure followed in the present work to select the working values (as presented in Table 2) of the numerous process parameters in hybrid CMT - P-GMAW NGW of mild steel material. The impact of process parameters on the weld arc stability and the joint quality is studied using the synchronously recorded instantaneous welding current, voltage, and high-speed arc images. The related details are presented in the results and discussion section. Wire cut EDM process is used to extract metallography samples from the weld plates. Subsequently, these samples are mirror polished using the grit papers of 80 to 2000 size in sequence, followed by cloth polishing in the diamond suspension of particle size 0.25 µm. Further, these polished samples are etched using a 2% Nital solution with a dwell time of 10 s. Macrographs are recorded using a stereomicroscope at 12.5X magnification. Micro images are captured at 500X magnification for every 1x1 mm array distance within the weld bead. The volume fractions of different phases in the weld joint are calculated using the point count method following the ASTM E562 standard [17]. The weld mechanical behavior is studied from microhardness and tensile tests following ASTM E384 and ASTM E8M standards, respectively [18, 19].

Heat input is determined by using recorded I-V characteristics for all the experiments. The average power and heat input of each cycle is computed as per Eqs. 1 and 2, respectively. A process efficiency (η) of 0.8

is used in the present work.

$$Power\ (P) = \frac{\sum_{i=0}^{n} I_i V_i t_i}{\sum_{i=0}^{n} t_i} (1)$$

Where *I*, *V*, and are welding current, voltage, and process efficiency, respectively.

$$HeatInput = \frac{P}{Weldingspeed} (2)$$

Table 2
Welding process parameters

Pass	Process	I_P (A)	t_P (ms)	I_b (A)	I_m (A)	Voltage (V)	Pulse frequency (Hz)	Welding speed (mm/s)	Heat input (J/mm)
Root pass	CMT	–	–	–	200	18 ± 0.2	80	5.4	479 ± 4
Filling and closing passes	P-GMAW	435	1.5	235	299	27 ± 1	180		827 ± 3
		360	5.0	235	275	27 ± 1	55	9.0	746 ± 4
		385	16.5	175	291	27 ± 1	30		816 ± 1

Other constant process parameters: number of passes – 4; narrow gap – 5 mm; Torch weaving amplitude – 1 mm; Torch oscillation frequency – 7 Hz; wire feed speed – 8.3 m/min.

3. Results and discussion

Figure 3(a) shows the influence of GMAW variants – CMT and P-GMAW on the behavior of weld arc and bead formation during the NGW of mild steel plates. Figure 3(b) depicts the real-time recorded current-voltage waveform of the CMT process. The arc images during the arcing phase [point 1 in Fig. 3(b)] and short-circuiting phase [point 2 in Fig. 3(c)] during the root pass welding is shown in Fig. 3(c,d), respectively, and the corresponding macrograph is presented in Fig. 3(e). Similarly, the arc images during the arcing and short-circuiting phase during the second pass deposition are shown in Fig. 3(f,g), and Fig. 3(h) depicts the corresponding macrograph. Figure 3(i) illustrates the real-time recorded current-voltage waveform of the P-GMAW process during the NGW of mild steel material. The arc images during the peak current [point 1 in Fig. 3(i)] and base current phase [point 2 in Fig. 3(i)] during the root pass welding are shown in Fig. 3(j,k), respectively, and the corresponding macrograph is presented in Fig. 3(l). Similarly, the arc images during the peak current and base current phases during the second pass deposition are shown in Fig. 3(m,n), and Fig. 3(o) depicts the corresponding macrograph.

A complete sidewall fusion was evident in the case of root pass welding for both CMT and P-GMAW, and this can be related to the enhanced flow of arc and molten pool to the side walls due to the circular

groove in the backing plate. Incomplete side wall fusion is evident after the second pass deposited with the CMT process, while improved side wall fusion is observed with the P-GMAW weld bead. The incomplete side wall fusion in the CMT can be correlated to the lower arcing time and heat input associated with this process, where the droplet detachment takes place mainly due to the mechanical motion of the welding wire rather than the pinching forces related to the case of P-GMAW.

Figure 4 shows the influence of narrow gap distance on the welding arc behavior and the weld bead formation during the NGW. As per the observation from Fig. 3, the root pass is deposited using the CMT process, and the filling and closing passes are deposited using the P-GMAW process [Fig. 4(a)]. The narrow gap distance is changed at three levels – 5 mm, 6.5 mm, and 8 mm [Fig. 4(a)]. Figure 4(b-g) shows the arc images in the narrow gap maintained at a distance of 5 and 8 mm, respectively. The deflected arcs during the electrode oscillation to the left and the right faying surface are shown in Fig. 4(b) and (d) for a 5 mm narrow gap distance and Fig. 4(e) and (g) for 8 mm. The welding arc is stable in the narrow gap center [Fig. 4(c) and (f)] while the arc climbs the faying surface as it approaches the side wall [Fig. 4(b), (d), (e), and (g)]. The sudden jump of the arc from the narrow gap center to the side walls results in the loss of arc stability. The increase in the unstable arc region with the decrease in the narrow gap distance diminishes the side wall fusion in the weld joint, as shown in Fig. 4(h) and (i). Figure 4(j) depicts the weld joint with no defects with a larger narrow gap distance. However, the increase in the narrow gap distance enhances the volume of filler material, resulting in higher heat input and a reduction in the weld joint mechanical properties. Also, it increases the total welding time, directly affecting the production rates. This work considers the narrow gap distance of 5 mm for further studies.

Figure 5 shows the influence of torch/arc oscillation on the welding arc behavior and the weld bead formation during the NGW. As per the observations from Figs. 3 and 4, the root pass is deposited using the CMT process, and the filling and closing passes are deposited using the P-GMAW process. Further, the narrow gap distance is maintained constant at 5 mm. The torch/arc oscillation varies at three levels – 0.0, 1.0, and 2.0 mm [Fig. 5(a)]. Figure 5(b) shows the welding arc at 0 mm or no arc oscillation condition where a stable welding arc is positioned at the center of the narrow gap. The corresponding welding macrograph [Fig. 5(c)] depicts the incomplete fusion between the layers and the side wall. It is due to the non-reachability of the welding arc to the sidewall and the absence of high-intensity arc exposure to the corners. Figure 5(d,e) shows the arc images near the right and left faying surfaces during the 1 mm arc oscillation condition. Figure 5(f) explains the improvement in the interlayer melting and side wall fusion as the arc oscillations help move the arc from its mean position resulting in higher arc interactions with the corners. The increase in the arc oscillation amplitude further to 2 mm results in the uncontrollable climbing of the arc over the faying surfaces [Fig. 5(g-i)] causing incomplete side wall fusion and interlayer melting. For a 5 mm narrow gap, 1 mm arc oscillation amplitude shows a stable arc with minimum weld defects.

Figure 6 shows the impact of welding voltage on the welding arc behavior and the weld bead formation during the NGW. As per the observations from Figs. 3–5, the root pass is deposited using the CMT process, and the filling and closing passes are deposited using the P-GMAW process. Further, the narrow

gap distance and arc oscillation amplitude are maintained constant at 5 mm and 1 mm, respectively. The welding voltage was varied at three levels – 20 V, 25 V, and 30 V [Fig. 6(a)]. Figure 6(b) shows the welding arc at 20 V condition, where a high-intensity welding arc with a lower arc length is positioned at the center of the narrow gap. The corresponding welding macrograph [Fig. 6(e)] depicts the incomplete side wall fusion. It is due to the non-reachability of the welding arc to the sidewall and the absence of high-intensity arc exposure to the corners. Figure 6(d) shows the arc image at 30 V welding condition and the corresponding macrograph [Fig. 6(g)] depicts the incomplete fusion with the side wall. The long and expanded arc associated with higher welding voltage conditions causes the weld bead to widen at the top of the faying surface and reduces the welding arc exposure to the narrow gap corners. Figure 6(c) shows the arc image for the 25 V welding condition. The corresponding macrograph shown in Fig. 6(f) explains the improvement in the side wall fusion as the high-intensity welding arc is equally distributed to all the regions.

Figure 7 shows the influence of the number of passes on the welding arc behavior and the weld bead formation during the NGW. As per the observations from Figs. 3–6, the root pass is deposited using the CMT process, and the filling and closing passes are deposited using the P-GMAW process. Further, the narrow gap distance, arc oscillation amplitude, and welding voltage are maintained constant at 5 mm, 1 mm, and 20 V, respectively. The number of weld passes was varied at four levels – 1, 2, 3, and 4 [Fig. 7(a)]. A constant wire feed speed (WFS) with increased welding speed requires more passes to fill the joint. The set of welding speeds and the number of passes considered in the present work are presented in Table 3. Figure 7(b,c) shows the arc images and molten metal in the narrow gap at the welding conditions (4.2 mm/s, 2 passes) and (9 mm/s, 4 passes), respectively. The overhead flow of the molten pool was noticed in Fig. 7(b), which acts as a hindrance for the arc to strike the previously deposited layer. This results in the lack of side wall and interlayer fusion. The absence of overhead flow of the molten pool was observed with the simultaneous increase in the welding speed and number of passes (Fig. 7(c)), minimizing the lack of fusion defects. Figure 7(d-g) shows the weld macrographs of a single-pass, two-pass, three-pass, and four-pass weld joint, respectively, where the lack of side wall and interlayer fusion defects are reduced and can be directly correlated to the minimization of the overhead flow of the molten weld pool.

Table 3
Welding speeds and the number of passes

Number of passes	Welding speed (mm/s)	
	Root pass	Filling and closing passes
1	3	
2	5.4	4.2
3		6
4		9

To adopt the hybrid CMT - P-GMAW process to join the thick plates, it is recommended to choose the CMT process to deposit the root pass and the filling and closing pass with the P-GMAW process. Further, the welding voltage, narrow gap distance, arc oscillation amplitude, and the number of passes are recommended to be maintained constant at ~ 25 V, 5 mm, 1 mm, and four passes, respectively. The weld joint properties can be improved by choosing the suitable pulse frequency corresponding to P-GMAW. Emphasis is given subsequently to understanding the effect of P-GMAW pulse frequencies in the hybrid CMT - P-GMAW process on the arc behavior, molten metal transfer from the electrode, microstructure, and mechanical properties of the narrow gap joints of mild steel plates. Three different pulse frequencies and the related welding conditions, as presented in Table 2, are used to perform the experiments.

Figure 8 shows the synchronized high-speed arc images (1–14) corresponding to the points on instantaneous current and voltage waveforms for the higher pulse frequency of 180 Hz to demonstrate the arc behavior and molten electrode metal transfer phenomenon in the NGW of 12 mm thick steel plates. At point 1, the pulse current is 435 A, and the voltage is 29 V with a welding arc of high intensity. The arc is deflected towards the left faying surface of the wall where the welding electrode is at extreme left during torch oscillation. From point 2, the welding current and voltage dip to 235 A and 24 V in the background phase, where the deflection of the welding arc to the side wall decreases due to the relatively shorter arc associated with the lower voltages and the electrode movement towards the center. The one drop per pulse phenomenon can be noticed in points 3–5. The sequence of observations follows the melting of the electrode in point 3, the formation of the droplet pendant in point 4, and the one drop per pulse detachment in background current at point 5, followed by the completion of droplet transfer into the weld pool at point 6. Similar repeated phenomena are observed with every pulse cycle from point 7 to 14, during which the electrode shifts towards the right faying surface. The undeflected or straight welding arc can be observed at points 7–9, where the welding electrode is at the center during torch oscillation.

Observations from Fig. 8 are schematically represented in Fig. 9 for better visualization and understanding of the welding arc and molten metal transfer behavior for 180 Hz pulse frequency while the electrode moves from the left to the right side of the wall during the torch oscillation. Figure 9(a-b) shows the deflection of the welding arc towards the left side wall at 8 ms, followed by the welding arc moving to the center during the arc oscillation at 30 ms. Figure 9(c-d) shows the welding arc and droplet (one drop) detachment at 31 ms and the welding arc deflected towards the right side wall at 75 ms. The average arc length for a 180 Hz pulse frequency is 3.3 (± 0.4) mm.

Figure 10 shows the synchronized high-speed arc images (1–9) corresponding to the points on instantaneous voltage and current waveform for the pulse frequency of 55 Hz to demonstrate the arc behavior in the narrow gap joint. At point 1, the pulse current is 360 A, and the voltage is 31 V with a welding arc of high intensity. The arc is deflected towards the left faying surface of the wall where the welding electrode is at extreme left during weld arc oscillation. It is noted that 360 A pulse current and its durations of 5 ms increase the voltage, which leads to higher arc lengths. During this region, the deflected arc is in direct contact with the left side wall, and the deflection to the side wall is much higher than that of the 180 Hz pulse frequency condition. The droplet detachment in the pulse current was noticed due to

longer pulse current durations at point 2, contrary to the 180 Hz condition. From point 3, the welding current and voltage dip to 235 A and 26 V, respectively, in the background phase, where the deflection of the welding arc to the side wall decreases as the torch moves toward the center. The multiple droplets per pulse phenomenon can be observed from points 4–6. The observation follows the melting of the electrode and multiple droplet detachment at point 4, a trace of droplets at point 5, followed by the low-intensity welding arc during the background current at point 6. Similar repeated phenomena are observed with every pulse cycle from points 7–9, during which the electrode shifts towards the right faying surface.

Similarly, observations from Fig. 10 are schematically represented in Fig. 11 for 55 Hz pulse frequency. Figure 11(a) shows the welding arc deflected towards the left side wall and the droplet detachment to the weld pool at 5 ms. Figure 11(b) shows the low-intensity welding arc during the background current region at 19 ms, where the welding arc shifts towards the center during the arc oscillation. The welding arc during the pulse current region where multiple droplet transfer can be observed at 23 ms, as shown in Fig. 11(c)—followed by the welding arc at the background current region at the center of the faying surface at time 38 ms as shown in Fig. 11(d). Figure 11(e) shows the welding arc at time 70 ms, where the welding arc is deflected towards the right-side wall and the droplet detachment to the weld pool. The average arc length for a 55 Hz pulse frequency is 4.84 (± 0.3) mm, 45% higher than that of the 180 Hz pulse frequency resulting in higher deflections towards the side wall.

Figure 12 shows the synchronized high-speed arc images (1–14) corresponding to the points on instantaneous voltage and current waveform for 30 Hz pulse frequency. At point 1, the pulse current is 385 A, and the voltage is 31 V with a welding arc of high intensity. The arc is deflected towards the left faying surface of the wall where the welding electrode is at extreme left during weld arc oscillation. It is noted that 385 A pulse current and its durations of 16.5 ms increase the voltage, which leads to higher arc lengths. During this region, the deflected arc is in direct contact with the left side wall, and the deflection to the sidewall is much higher compared to 180 Hz and 55 Hz pulse frequency conditions. Droplet formation due to high welding current and longer pulse phase is noticed at point 2, pinching of the droplet from the wire, droplet detachment, and following the streaming mode of droplet detachment were seen in points 3–5. Small droplet detachment was visible in the background current durations at points 6–8, where the welding arc is at the center of the faying surfaces during torch oscillation. Similar repeated phenomena are observed with every pulse cycle from point 9 to 14, during which the electrode shifts towards the right faying surface.

Similar to previous explanations, Fig. 13 shows the schematic representation of the observations for 30 Hz pulse frequency. The average arc length at this frequency is measured as 4.95 (± 0.6) mm, 48.6% and 3% higher than that of the 180 Hz and 55 Hz pulse frequency conditions, respectively. As a result, the arc deflection towards the side wall is relatively more, as shown in Fig. 13(a and f). Figure 13(b-d) shows the droplet's formation and detachment followed by the streaming mode of metal transfer during the pulse cycle at 15, 17, and 19 ms, respectively. During this period, the welding arc is at the center of the faying surfaces during arc oscillation. Figure 13(e) shows the schematic representation of a low-intensity

welding arc during background current duration at 28 ms, where the welding electrode starts shifting towards the right faying surface during torch oscillation.

Figure 14(a-c) shows the transverse weld macrographs of the narrow gap weld joint produced using the pulse frequency of 180 Hz, 55 Hz, and 30 Hz, respectively. The complete side wall fusion is evident for all the pulse frequencies considered in the present work. The weld penetration dimensions are calculated from a fixed reference, i.e., from the top surface of the plate. The penetration of pass 2 (~ 8.5 mm) and pass 3 (~ 6.2 mm) for all the pulse frequencies is the same. However, there is a noticeable change in the final pass weld penetration, width, and reinforcement. The 30 Hz, pulse frequency condition, produced 20% higher weld penetration, 20% less reinforcement, and 14% less weld reinforcement width than the other two frequencies in the final pass. The higher penetration in 30 Hz pulse frequency may be owing to the relatively long pulse duration, resulting in more penetration in the last pass, which contrasts from passes 2 and 3, where the peak current heat is deflected to faying surfaces.

Figure 15(a) indicates the ferrite (white), and perlite (dark) in a base metal microstructure, and the same is depicted in the SEM picture for distinct visualizations of the phases present, as shown in Fig. 15(b). The weld metal microstructures displayed in Fig. 15(c and d) contain grain boundary ferrite (α_{Gb}), Widmanstatten ferrite (α_w), polygonal ferrite (α_P), and acicular ferrite (α_A). The martensitic microstructure with prior austenite grain boundaries is noticed in the HAZ region, as shown in Fig. 15(e and f).

Figure 16 depicts the influence of pulse frequencies on the volume fraction of ferrite phases formed in the weld pool. It is observed that the volume fraction of the acicular ferrite phase is higher (α_A = 86.8%, α_{Gb} = 11.3%, and α_W = 1.9%) in the case of 30 Hz pulse frequency condition followed by 55 Hz pulse frequency condition (α_A = 80.6%, α_{Gb} = 16.8%, and α_W = 2.6%) and then 180 Hz pulse frequency condition (α_A = 77.6%, α_{Gb} = 20.8%, and α_W = 1.6%). The higher volume fraction of the acicular ferrite phase in 30 Hz is due to the longer background current duration (16.5 ms). The liquid metal was undercooled in this region when the heat input was suddenly reduced. This helps in localized heterogeneous nucleation, which leads to grain refinement and easy formation of the acicular ferrite phase [20, 21]. The same effect is also noticed in the 55 Hz pulse frequency condition, but a relatively less volume fraction of the acicular ferrite phase is observed when compared to the 30 Hz pulse frequency due to lower background current durations (13 ms). The further reduction in the background current duration (5 ms) associated with 180 Hz pulse frequency decreases the volume fraction of the acicular ferrite phase to the minimum compared to the other welding conditions.

Hardness profiles were taken at three levels in the thickness direction, i.e., 2, 6, and 10 mm from the top surface of the base plate. Figure 17(a-c) shows the hardness profiles for the 180 Hz, 55 Hz, and 30 Hz pulse frequency conditions in narrow gap weld joints. The profile covers the weld metal, heat-affected zone (HAZ), and base metal. It can be seen that the microhardness values are higher in HAZ for all the pulse frequencies. The weld metal average microhardness values for 180 Hz, 55 Hz, and 30 Hz pulse frequency conditions are 213 (± 12) HV, 223 (± 9) HV, and 221 (± 10) HV, respectively. The hardness distribution shown across the weldment at a distance of 6 mm from the top surface of the base metal is

lower when compared to the 2 mm and 10 mm regions. This is due to the exposure of this 6 mm region to multiple thermal cycles (passes 3 and 4). The HAZ hardness is higher than weld metal due to the martensitic structure formed in the microstructures [Fig. 17(e and f)].

Figure 18 depicts the influence of pulse frequencies on weld joint tensile properties. The maximum yield strength, tensile strength, and lower percentage elongation (474 MPa, 596 MPa, 15%) were noticed in the 30 Hz pulse frequency condition. In contrast, minimum yield strength, tensile strength, and higher percentage elongation (349 MPa, 504 MPa, and 19%) were noticed in the 180 Hz pulse frequency condition. This is attributed to a higher percentage of acicular ferrite (86.8%) at 30 Hz and a comparatively lower percentage of acicular ferrite (77.6%) in the case of the 180 Hz pulse frequency condition. Similarly, these mechanical properties (373 Mpa, 534 Mpa, and 18%) for the 55 Hz pulse frequency fall between 30 and 180 Hz due to the intermediate acicular ferrite (80.6%) formation.

4. Conclusions

The present work reports the NGW of mild steel plates using novel hybrid CMT – P-GMAW and systematic studies to understand the influence of associated process parameters on arc behavior, molten metal transfer phenomenon, and weld quality. The crucial observations are summarized as follows:

1. The welding arc's stability inside the narrow gap is primarily determined by process parameters such as narrow gap distance, welding arc oscillation amplitude, welding voltage, and the number of passes. Reducing narrow gap distance, increasing arc oscillation amplitude, and increasing welding voltage results in severe arc climbing over the faying surface, insufficient fusing between the layers, and incomplete side wall fusion. The overhead flow of the molten pool formed while simultaneously decreasing the number of layers and welding speed restricts heat transfer from the arc to the previously deposited layer, resulting in a lack of fusion.
2. For a constant wire feed rate and heat input, a higher pulse current and a shorter pulse time result in one drop per pulse. Increasing the pulse current duration (5 ms) results in the formation of multiple droplets as the pinching effect continues. Further enhancing the pulse current duration results in the streaming mode of metal transfer. Pulsing frequencies of 180 Hz, 55 Hz, and 30 Hz result in one drop per pulse, multiple droplets per pulse, and streaming mode, respectively.
3. The imposition of several thermal cycles in filling pass weld region reduces hardness compared to the root and cap passes. The higher hardness in the HAZ can be associated with the martensitic weld structure. A higher percentage of acicular ferrite is formed at a 30 Hz pulse frequency followed by 55 Hz resulting in higher weld joint tensile properties. Superior joint tensile strength is observed at 30 Hz pulse frequency followed by 55 Hz pulse frequency, while the joint tensile strength was relatively low at 180 Hz pulse frequency.
4. For a mild steel material of 12 m thickness, a sound weld joint with optimal heat input is accomplished by employing CMT for the root pass and P-GMAW for the filling and closing passes with a narrow gap distance of 5 mm, weld arc oscillation amplitude of 1 mm, welding voltage of 25 V, four number of weld passes (including the root pass) and 30 Hz pulse frequency. These

parameters can be adapted to the narrow gap joining of mild steel material of any plate thickness by varying the number of passes.

Declarations

Funding - This work was supported by the Naval Research Board, India (Grant number NRB/4003/PG/436), and Science and Engineering Research Board, India, (Grant numbers [CRG/2020/005089] and [SB/S2/RJN-093/2015]). Venkata Kiran Degala has received research support from above grants.

Competing Interests The authors declare no competing interests.

Author contribution - Sudheer Kumar Polamuri: conceptualization, methodology, investigation, validation, formal analysis, writing – original draft, visualization; Venkaiah Nasina: conceptualization, writing – review & editing, resources, supervision; Basu Biswajyoti: conceptualization, writing – review & editing, resources; Vinay Deshmuk: conceptualization, writing – review & editing, resources; Venkata Kiran Degala: conceptualization, methodology, investigation, formal analysis, resources, supervision, writing - review & editing, visualization, project administration, and funding acquisition.

Ethics approval - Not applicable

Consent to participate - Not applicable

Consent for publication - Not applicable

Conflict of interests - The authors declare that they have no known competing financial interests or personal relationships that could have appeared to influence the work reported in this paper.

References

1. Agrawal BP, Ghosh PK (2010) Thermal modeling of multipass narrow gap pulse current GMA welding by single seam per layer deposition technique. Mater Manuf Process 25:1251–1268. https://doi.org/10.1080/10426914.2010.489593
2. Agrawal BP, Ghosh PK (2017) Characteristics of Extra Narrow Gap Weld of HSLA Steel Welded by Single-Seam per Layer Pulse Current GMA Weld Deposition. J Mater Eng Perform 26:1365–1381. https://doi.org/10.1007/s11665-017-2516-y
3. Anant R, Ghosh PK (2017) Ultra-narrow gap welding of thick section of austenitic stainless steel to HSLA steel. J Mater Process Technol 239:210–221. https://doi.org/10.1016/j.jmatprotec.2016.08.016
4. Krampit AG, Krampit NY, Krampit MA (2014) Effect of the parameters of pulsed arc welding on the formation of a root layer in a narrow gap. Weld. Int. 28:629–630

5. Zhang G, Shi Y, Zhu M, Fan D (2017) Arc characteristics and metal transfer behavior in narrow gap gas metal arc welding process. J Mater Process Technol 245:15–23. https://doi.org/10.1016/j.jmatprotec.2017.02.006
6. Wang JY, Ren YS, Yang F, Guo HB (2007) Novel rotation arc system for narrow gap MAG welding. Sci Technol Weld Join 12:505–507. https://doi.org/10.1179/174329307X213756
7. Guo N, Wang MR, Guo W, et al (2014) Effect of rotating arc process on molten pool control in horizontal welding. Sci Technol Weld Join 19:385–391. https://doi.org/10.1179/1362171814Y.0000000203
8. Guo N, Han YF, Jia CB, Du YP (2011) Effects of wire rotating frequency on metal transfer process in rotating arc narrow gap horizontal GMAW. Adv Mater Res 189–193:3395–3399. https://doi.org/10.4028/www.scientific.net/AMR.189-193.3395
9. Liu G, Tang X, Xu Q, et al (2021) Effects of Active Gases on Droplet Transfer and Weld Morphology in Pulsed-Current NG-GMAW of Mild Steel. Chinese J Mech Eng (English Ed 34:. https://doi.org/10.1186/s10033-021-00583-2
10. Cai X, Fan C, Lin S, et al (2018) Optimization of shielding gas composition in narrow gap GMA welding based on response surface methodology. Int J Adv Manuf Technol 95:2405–2412. https://doi.org/10.1007/s00170-017-1373-z
11. Sun J, Nie P, Feng K, et al (2017) The elimination of pores in laser welds of AISI 304 plate using different shielding gases. J Mater Process Technol 248:56–63. https://doi.org/10.1016/j.jmatprotec.2017.05.011
12. Zhao Y, Shi X, Yan K, et al (2018) Effect of shielding gas on the metal transfer and weld morphology in pulsed current MAG welding of carbon steel. J Mater Process Technol 262:382–391. https://doi.org/10.1016/j.jmatprotec.2018.07.003
13. Wong YR, Ling SF (2014) An investigation of dynamical metal transfer in GMAW - Effects of argon shielding gas. J Mater Process Technol 214:106–111. https://doi.org/10.1016/j.jmatprotec.2013.08.003
14. Zhu L, Pan Y, Li Y (2012) Ultranarrow gap welding with constrained arc by flux strips. Adv Mater Res 472–475:2814–2818. https://doi.org/10.4028/www.scientific.net/amr.472-475.2814
15. Xu wanghui, Sanbao L, Chenglei F, Chunli Y (2012) Feasibility study on tandem narrow gap GMAW of 65 mm thick steel plate
16. Wang J, Sun Q, Zhang T, et al (2018) Arc characteristics in alternating magnetic field assisted narrow gap pulsed GTAW. J Mater Process Technol 254:254–264. https://doi.org/10.1016/j.jmatprotec.2017.11.042
17. Standard A (2008) Standard test method for determining volume fraction by systematic manual point count. ASTM E562-08
18. ASTM E384 (2002) Standard Test Method for Microindentation Hardness of Materials ASTM E384. ASTM Stand 14:1–24

19. ASTM E8 (2010) ASTM E8/E8M standard test methods for tension testing of metallic materials 1. Annu B ASTM Stand 4 1–27. https://doi.org/10.1520/E0008
20. Sharir Y, Pelleg J, Grill A (1978) Effect of arc vibration and current pulses on microstructure and mechanical properties of TIG tantalum welds. Met Technol 5:190–196. https://doi.org/10.1179/mt.1978.5.1.190
21. Kou S, Le Y (1988) Welding Parameters and the Grain Structure of Weld Metal - a Thermodynamic Consideration. Metall Trans A, Phys Metall Mater Sci 19 A:1075–1082. https://doi.org/10.1007/bf02628392

Figures

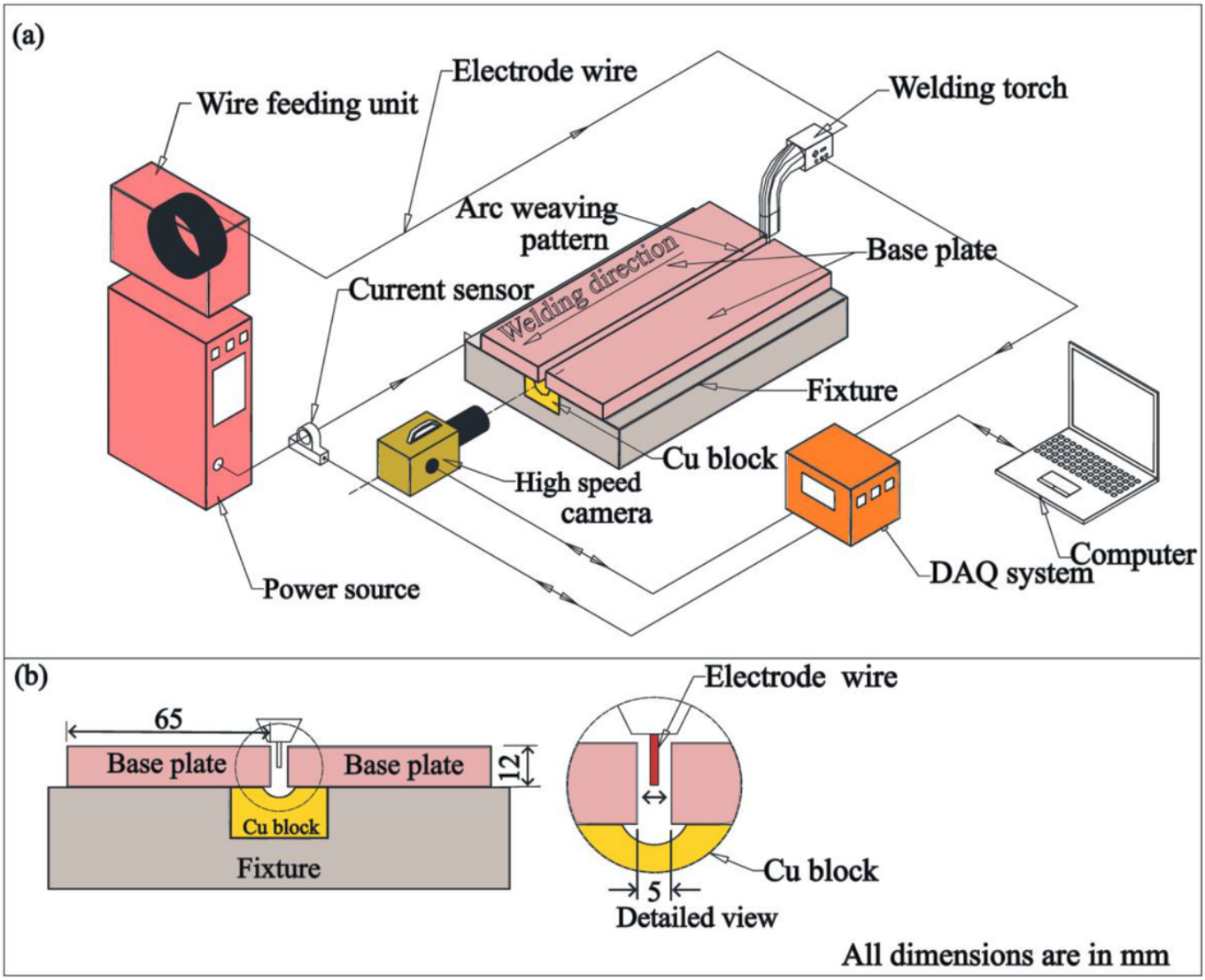

Fig. 1

Figure 1

Schematic representation of (a) gas metal arc welding setup, (b) weld joint configuration

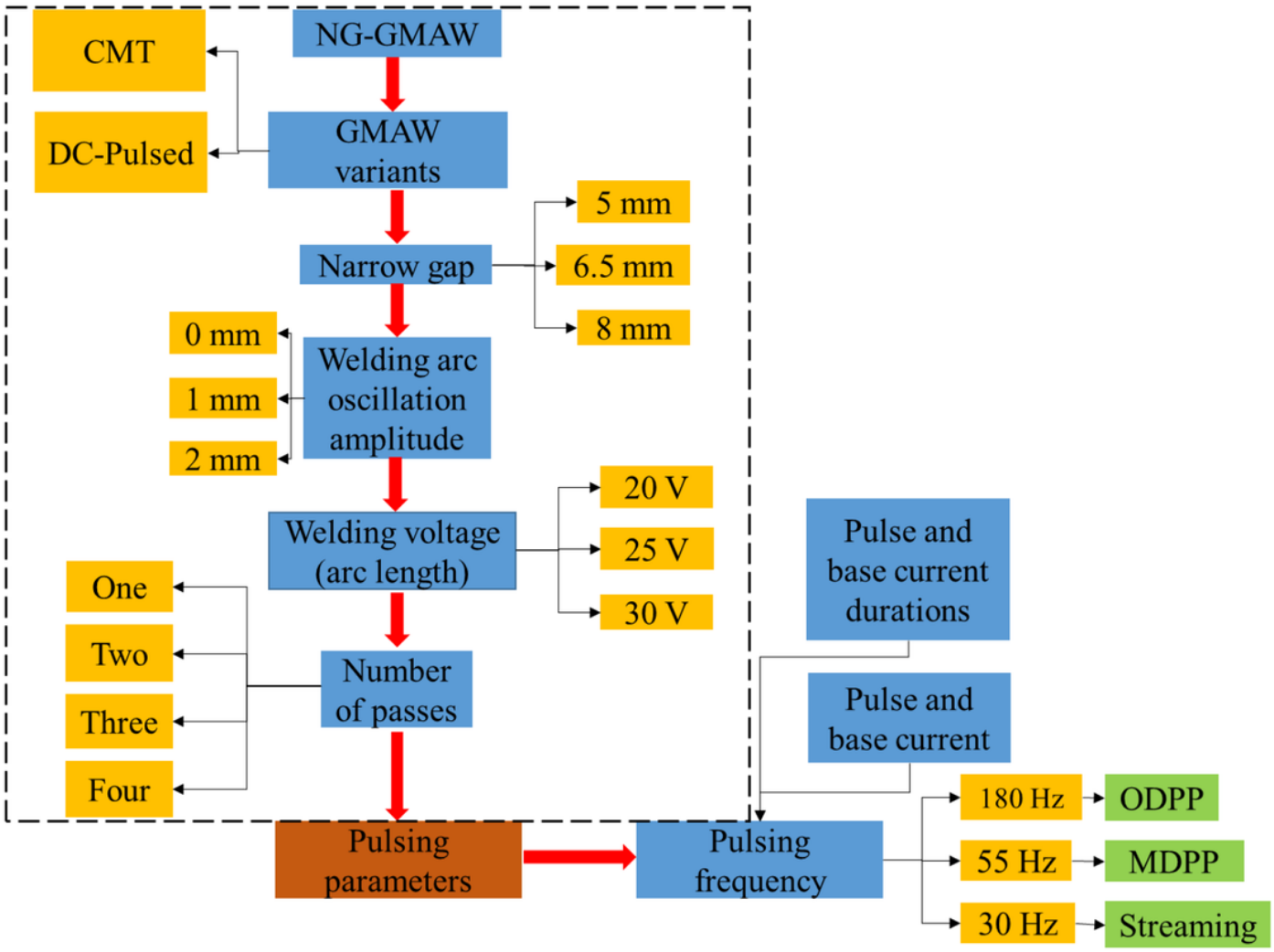

Fig. 2

Figure 2

Systematic experimentation followed in selecting the working values of numerous parameters in hybrid CMT - P-GMAW NGW of mild steel material

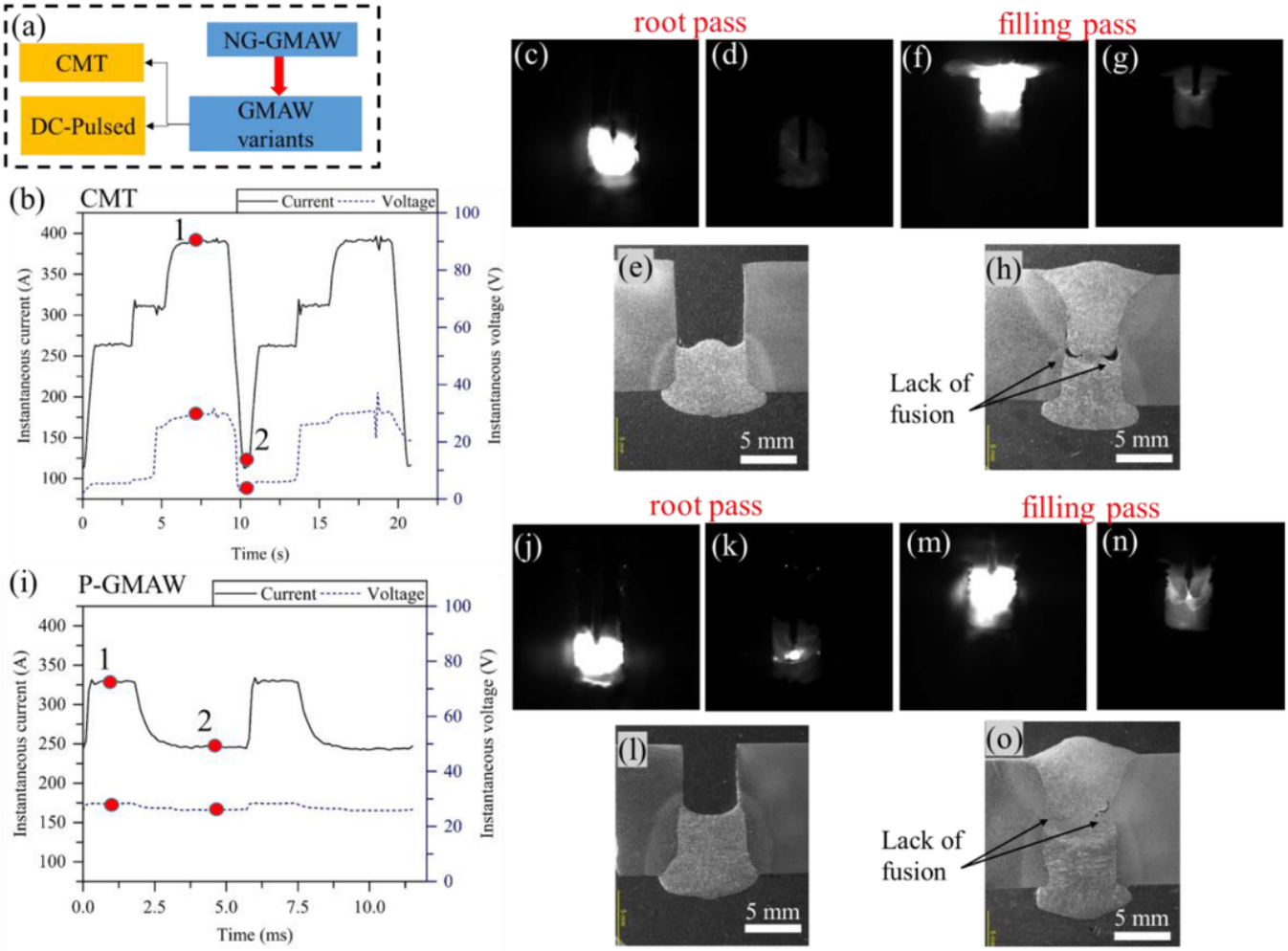

Fig. 3

Figure 3

Influence of GMAW variants on the weld joint quality

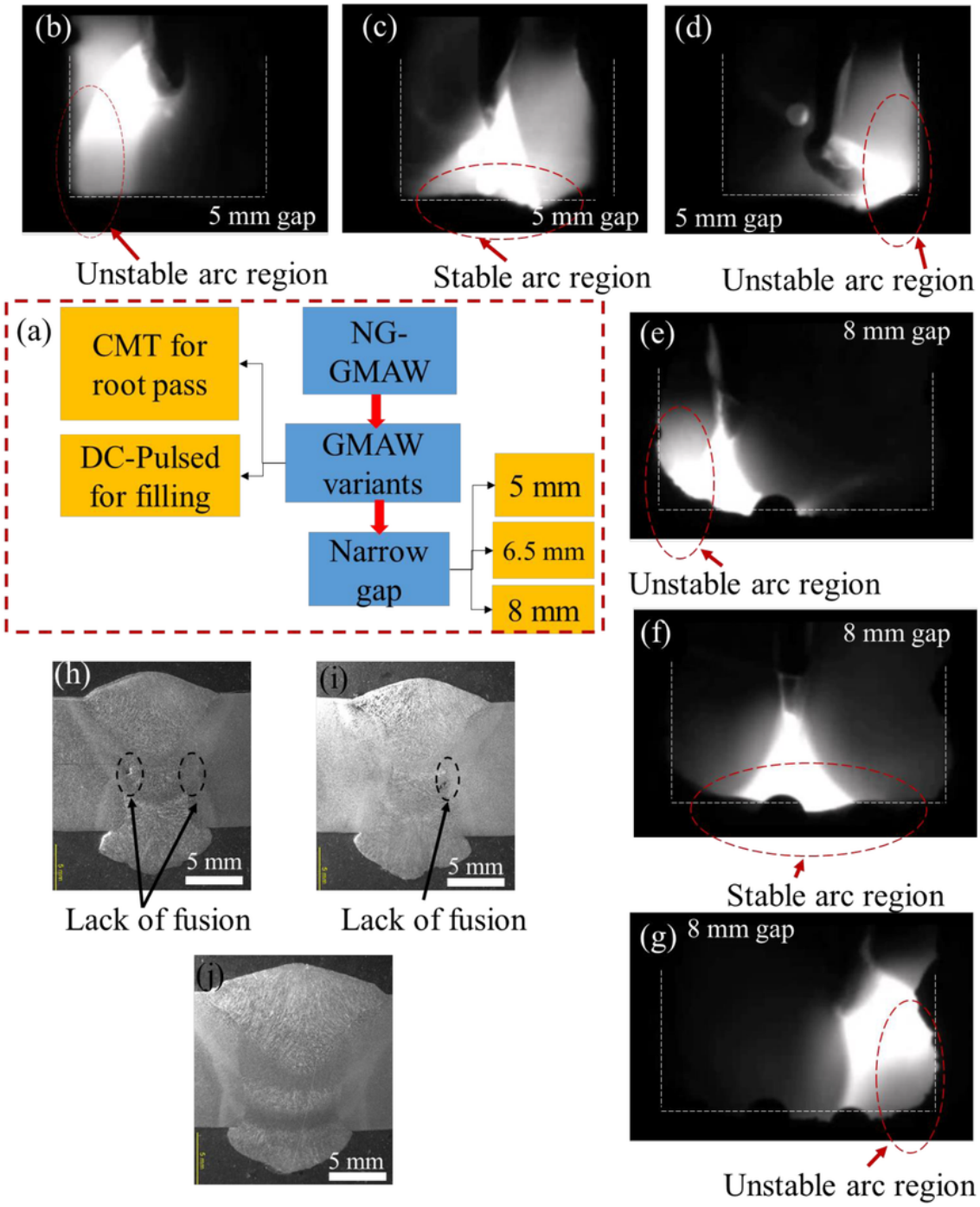

Fig. 4

Figure 4

Weld arc behavior and macrographs for narrow gap distance of 5, 6.5, and 8 mm joint gap

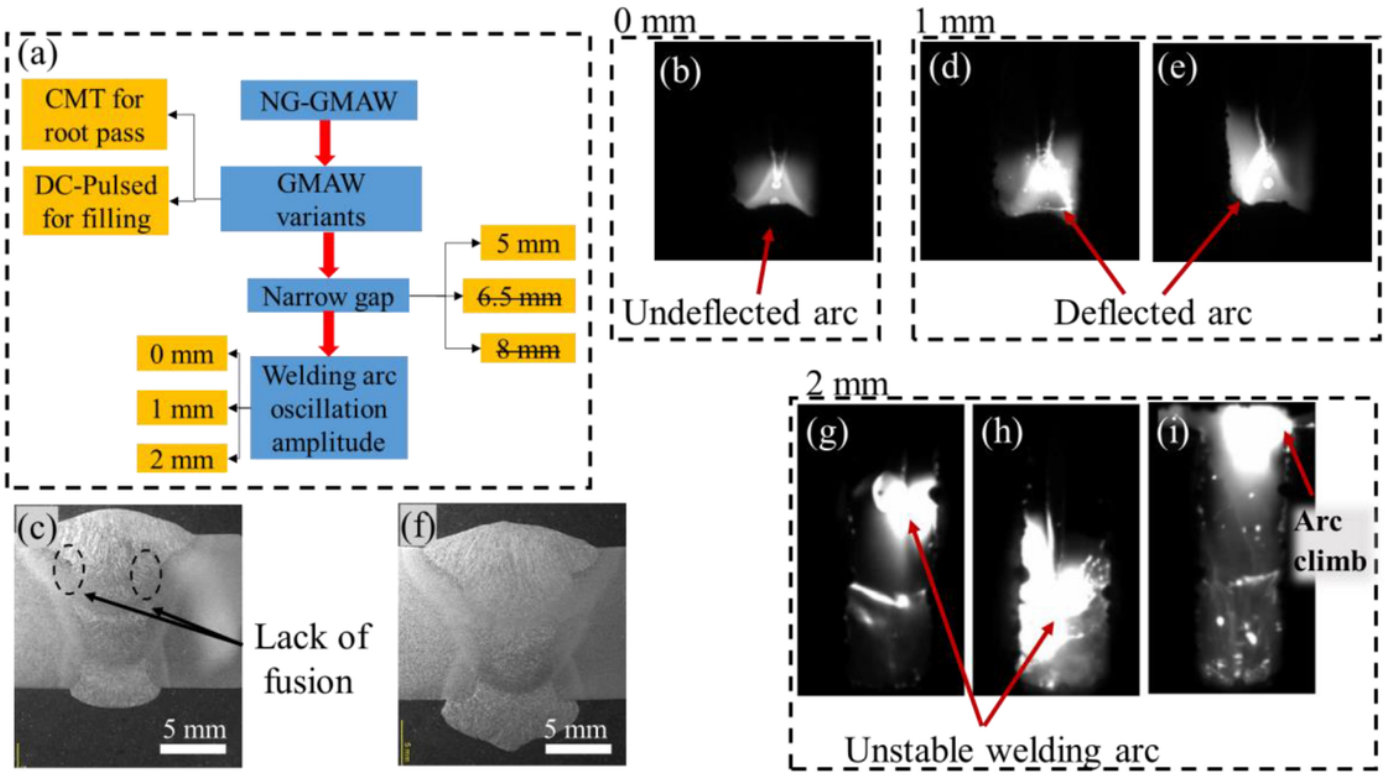

Fig. 5

Figure 5

Influence of weld arc oscillation on the stability of the arc and weld joint quality for a 5 mm narrow gap

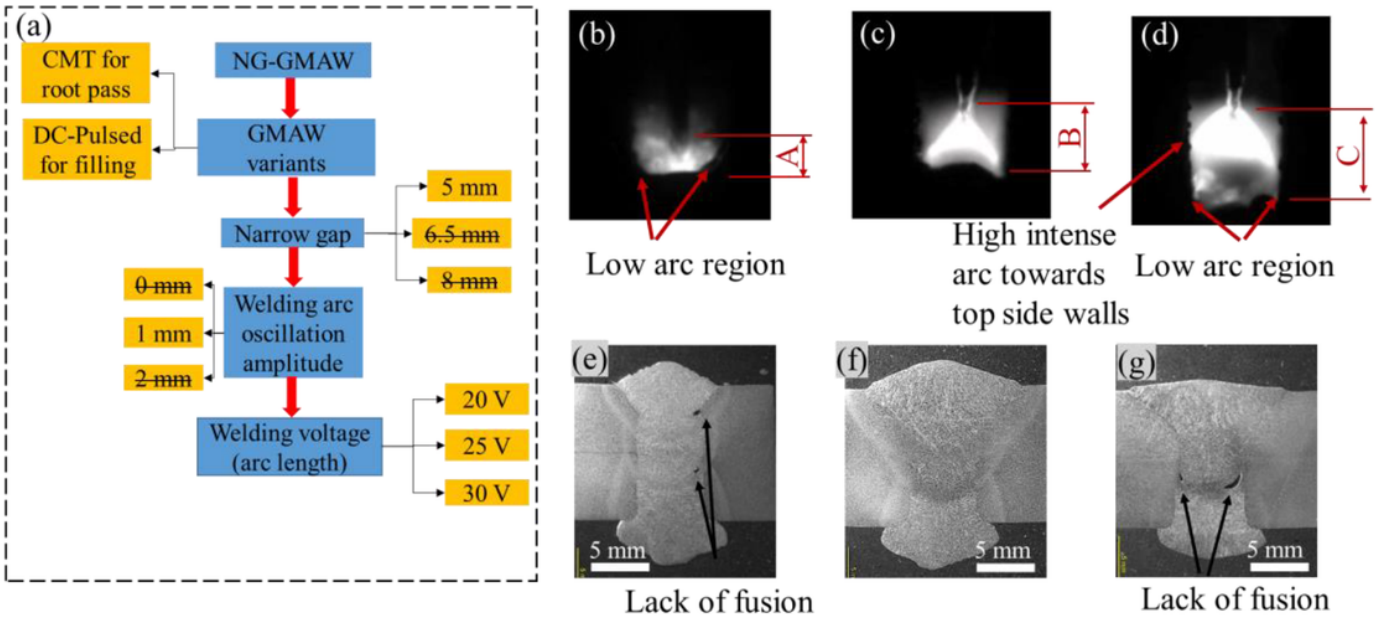

Fig. 6

Figure 6

Influence of welding voltage on the arc lengths and the weld joint quality

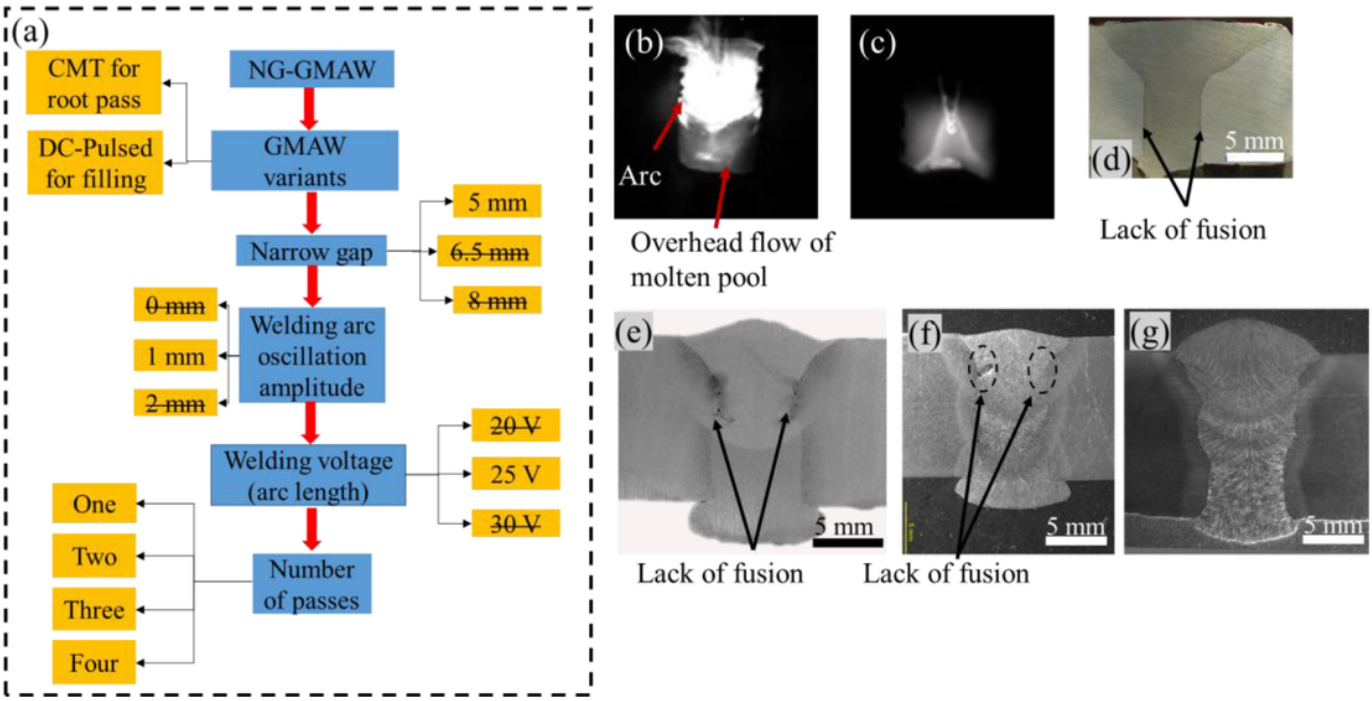

Fig. 7

Figure 7

Influence of the number of passes on the flow of molten pool inside the narrow gap

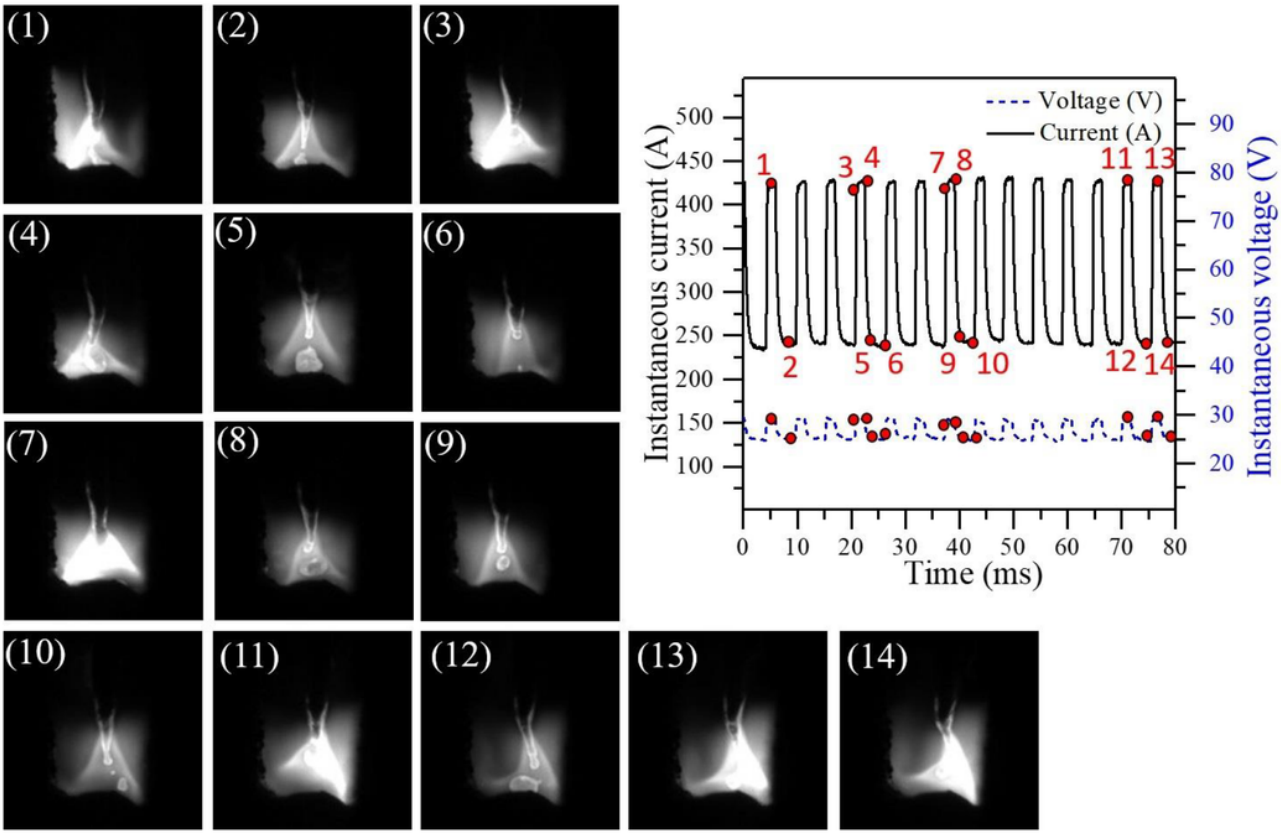

Fig. 8

Figure 8

Arc images depicting the welding arc and molten metal transfer phenomenon corresponding to real-time welding current and voltage for 180 Hz pulse frequency

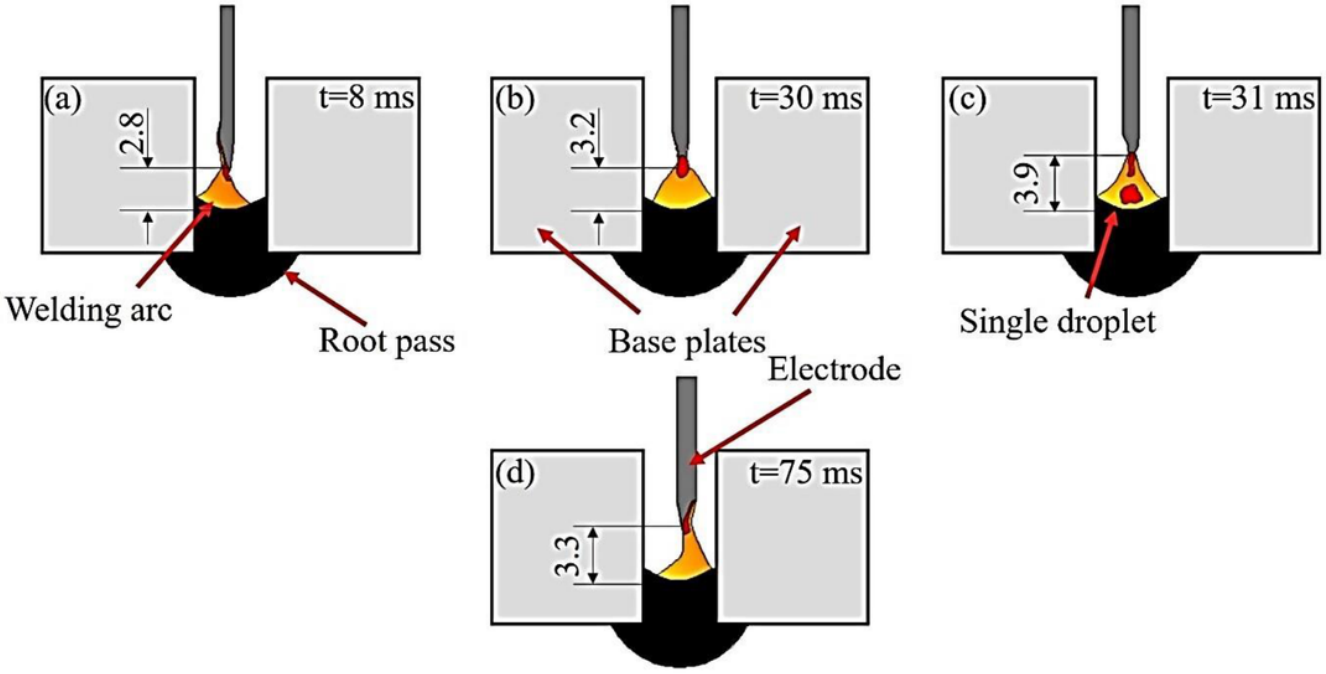

Fig. 9

Figure 9

Schematic diagram of arc and droplet detachment behavior for 180 Hz pulse frequency condition

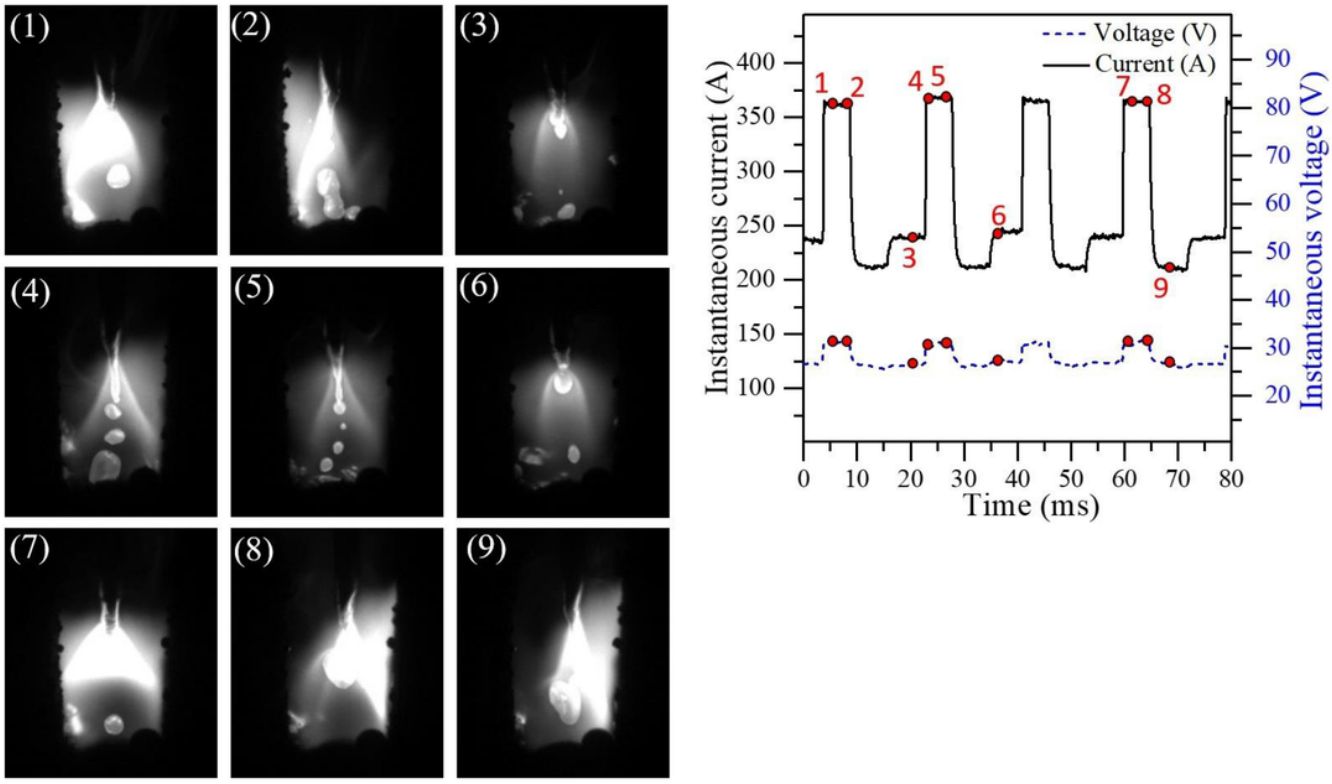

Fig. 10

Figure 10

Arc images depicting the welding arc and molten metal transfer phenomenon corresponding to real-time welding current and voltage for 55 Hz pulse frequency

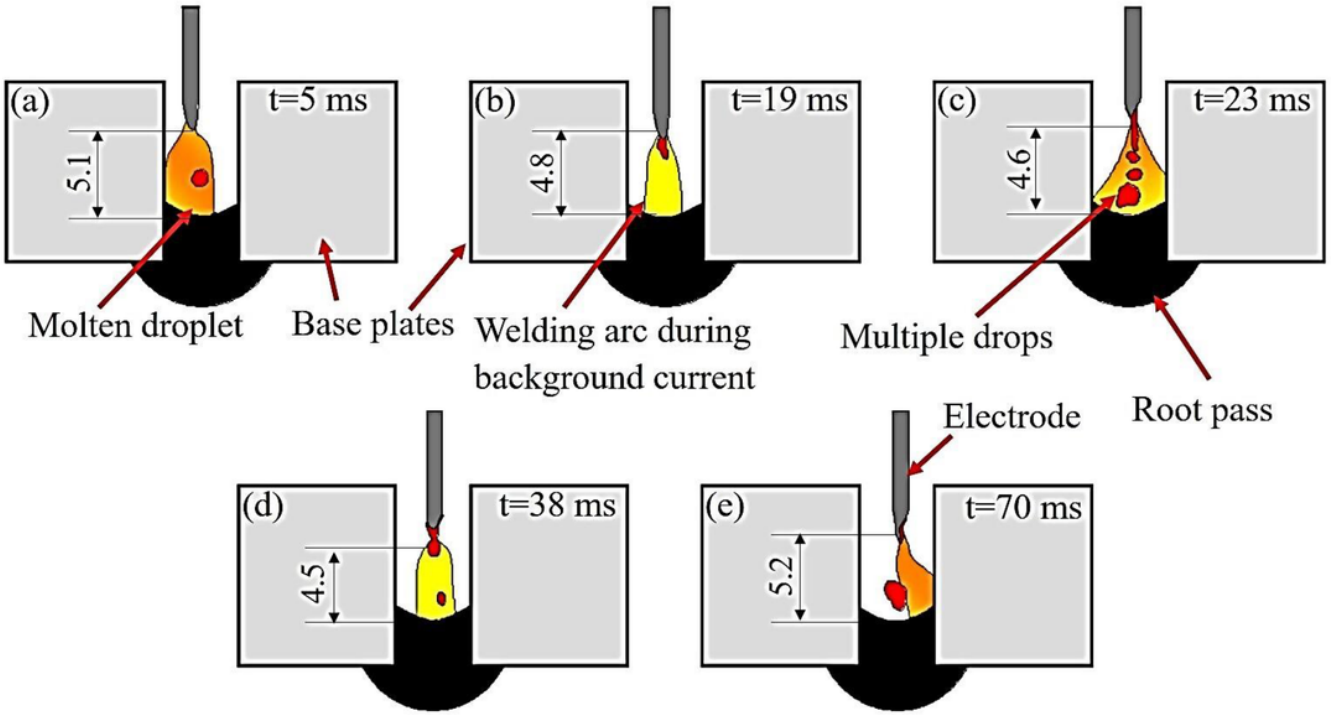

Fig. 11

Figure 11

The schematic diagram for the 55 Hz pulse frequency condition

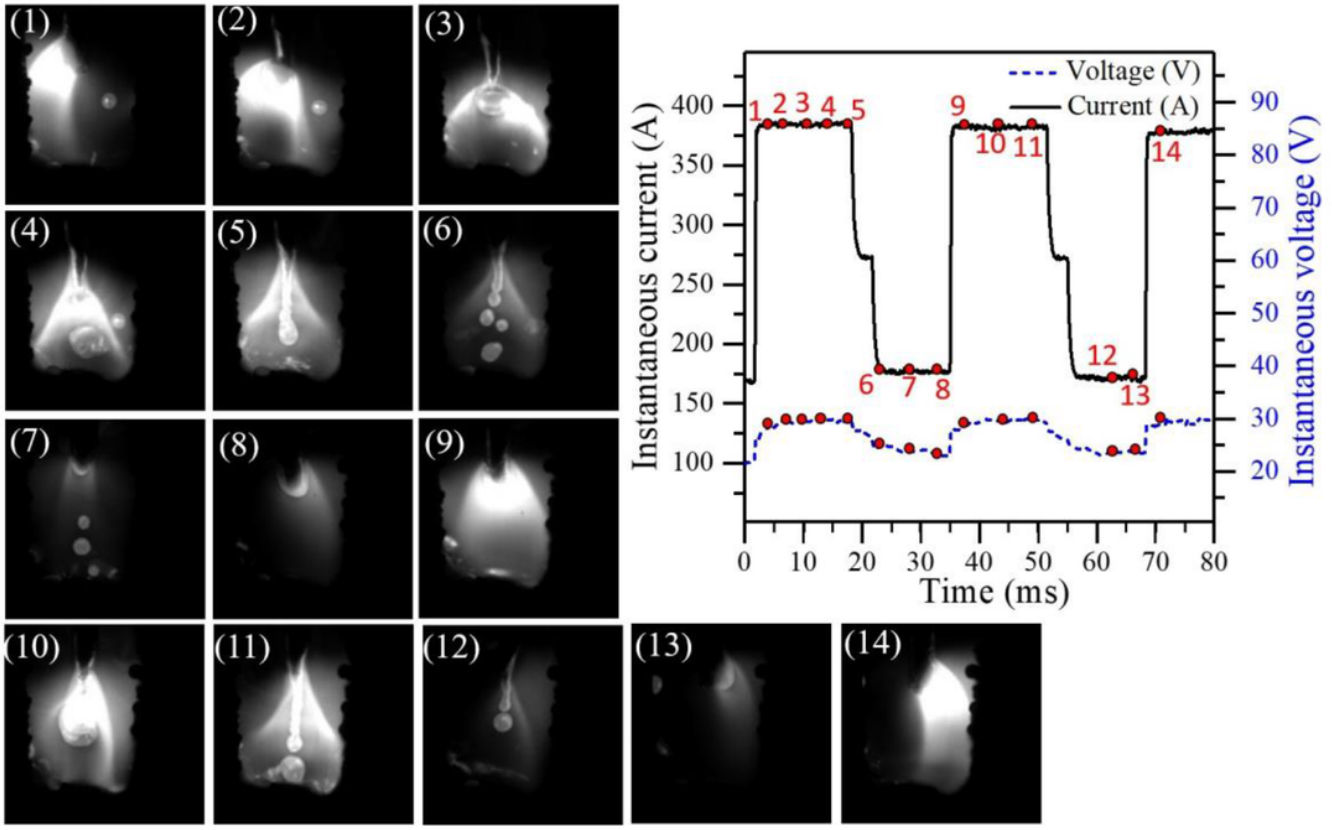

Fig. 12

Figure 12

Arc images depicting the welding arc and molten metal transfer phenomenon corresponding to real-time welding current and voltage for 30 Hz pulse frequency

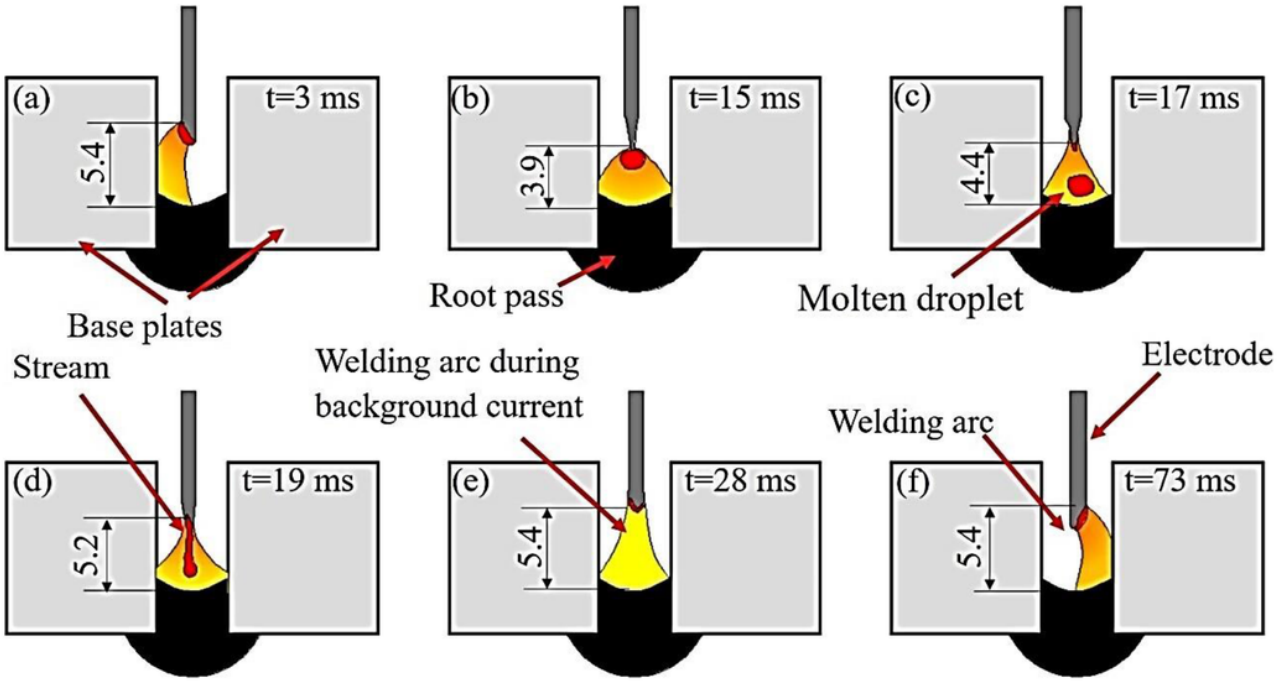

Fig. 13

Figure 13

The schematic diagram for the 30 Hz pulse frequency condition

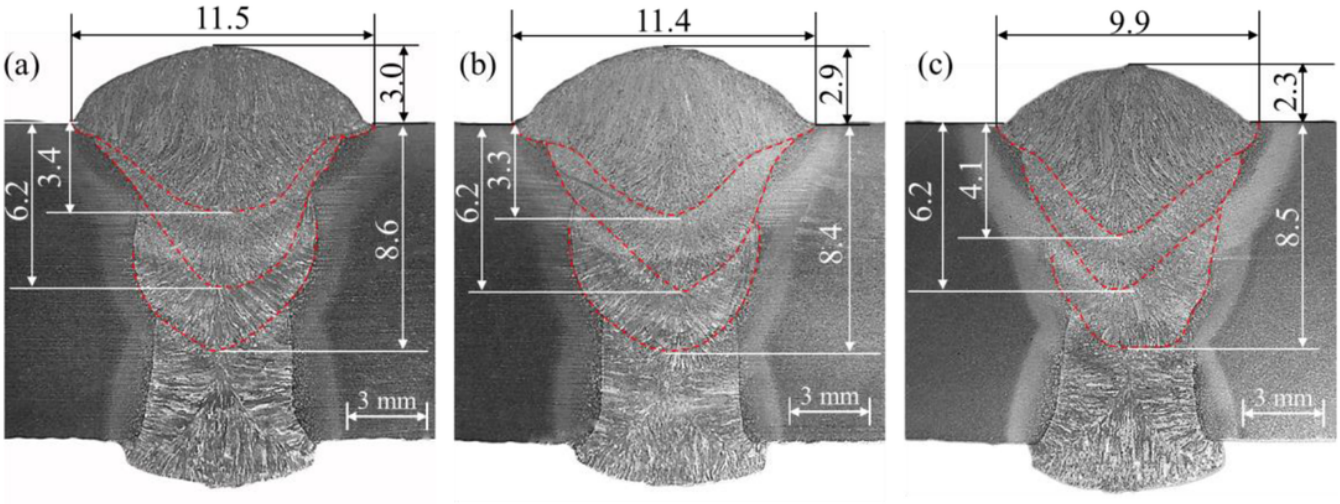

Fig. 14

Figure 14

Weld macrograph of NGW joint for pulse cycle frequencies (a) 180 Hz, (b) 55 Hz, and (c) 30 Hz

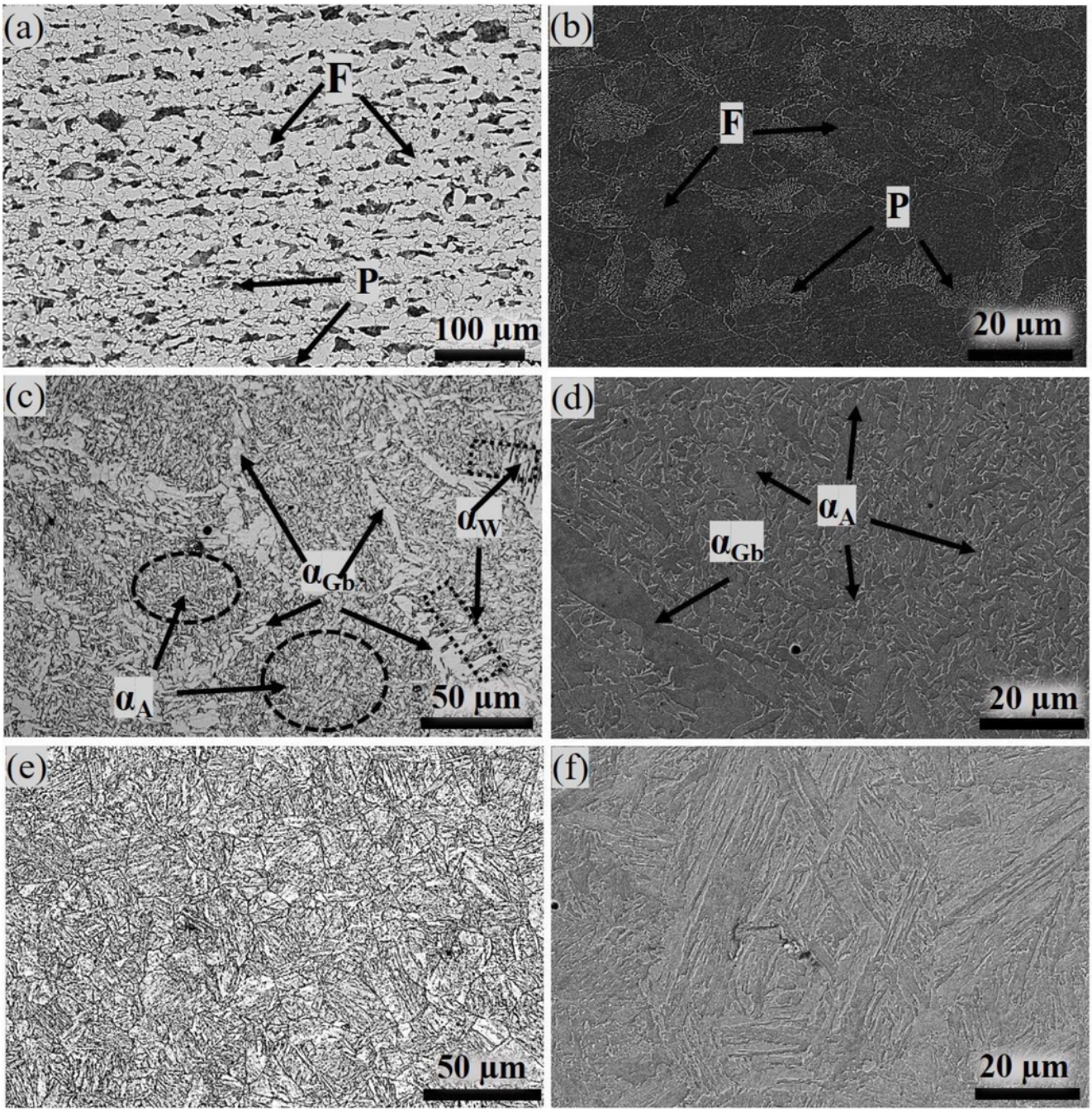

Fig. 15

Figure 15

Shows the optical micrographs (a) base metal microstructure, (b) base metal SEM image, (c) weld metal microstructure, (d) weld metal SEM image, (e) HAZ region, and (f) HAZ SEM image

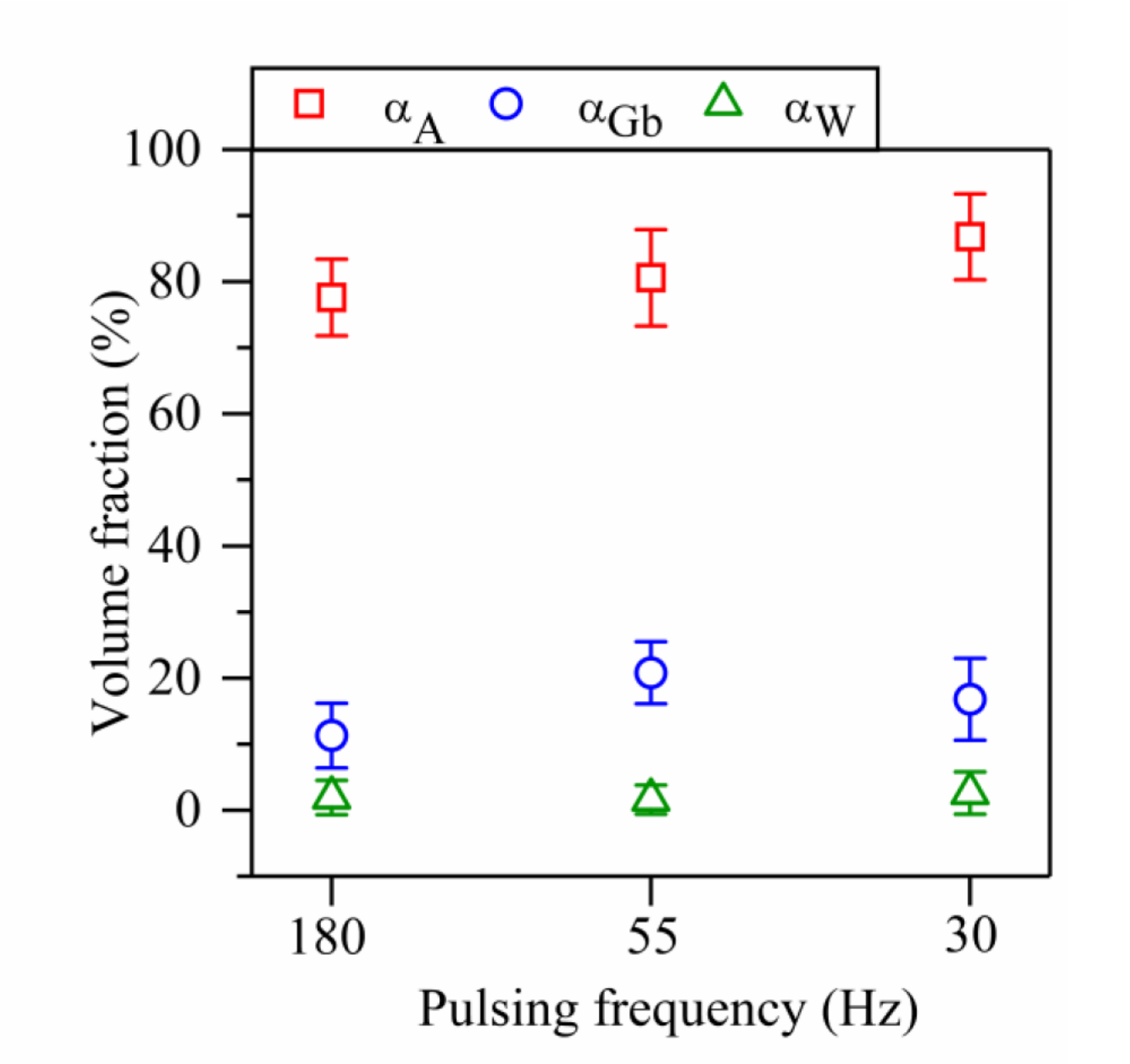

Fig. 16

Figure 16

Influence of pulse frequencies on the volume fraction of ferrite phases in the weld pool

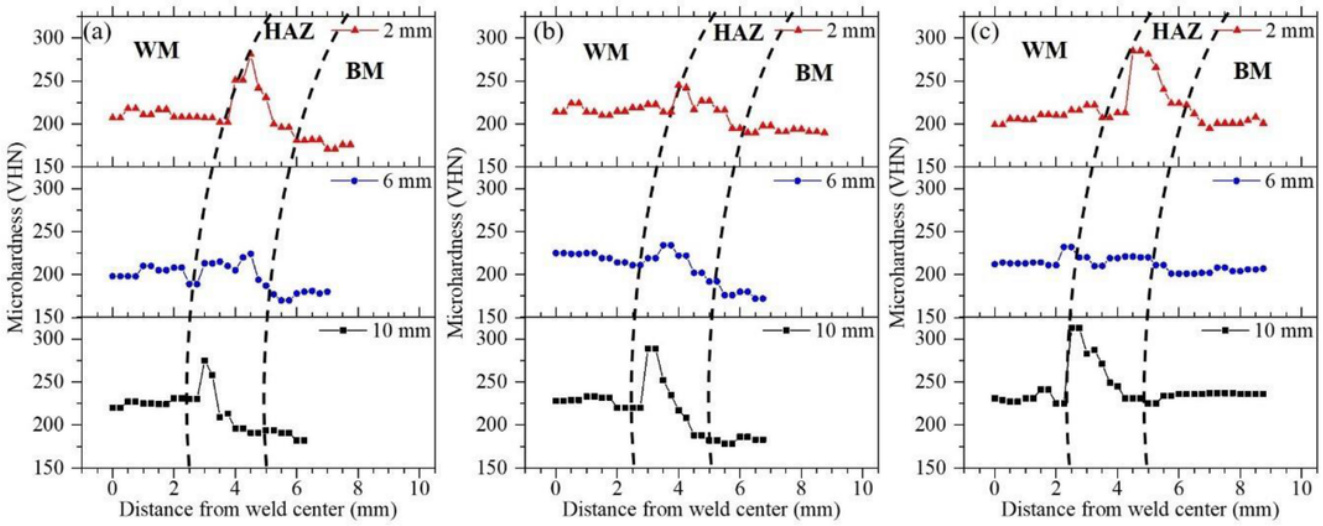

Fig. 17

Figure 17

Influence of pulse frequency on the microhardness for (a) 180 Hz, (b) 55 Hz, and (c) 30 Hz

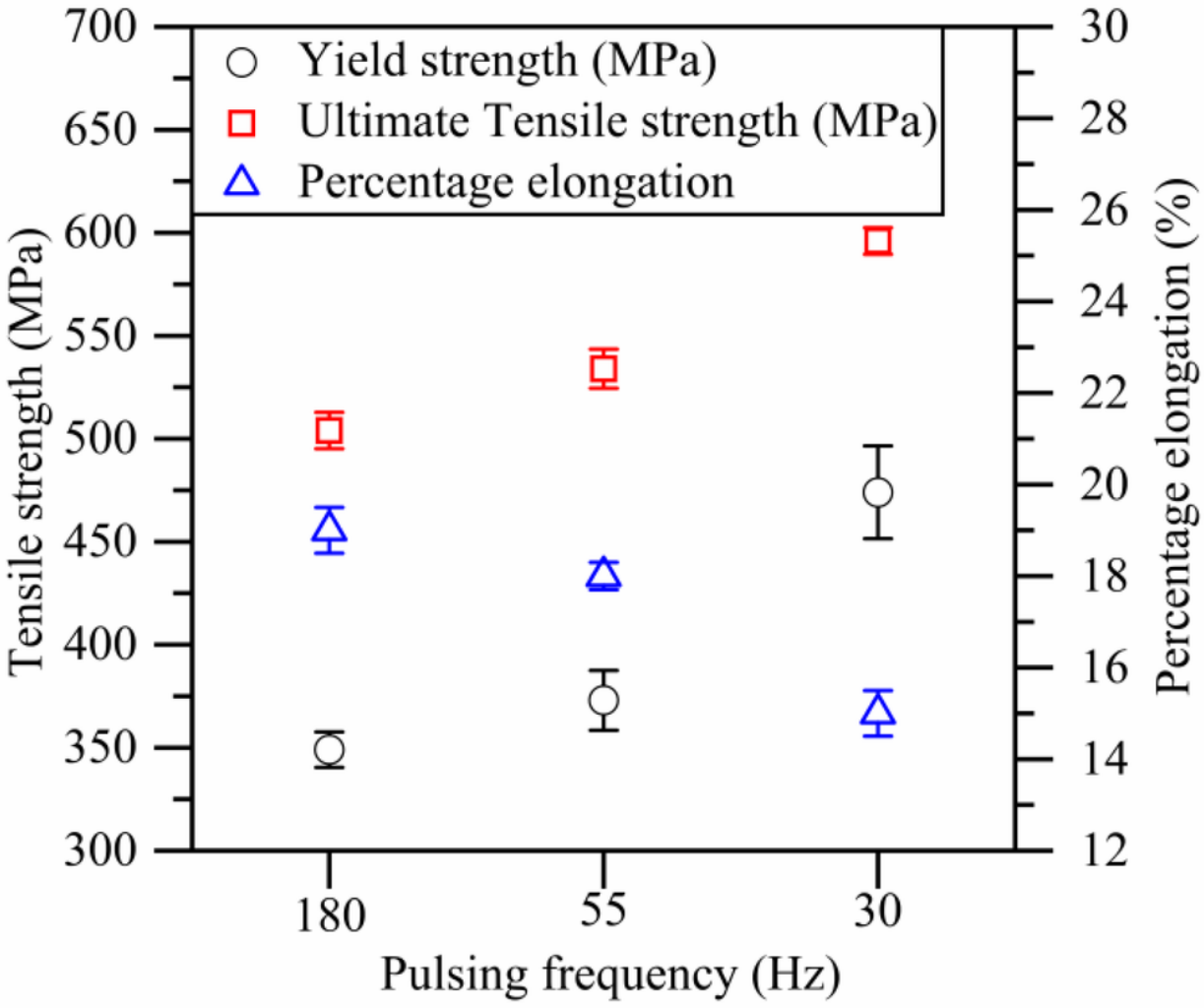

Fig. 18

Figure 18

Influence of pulse frequencies on weld joint tensile properties